American Mineralogist, Volume 77, pages 422–430, 1992

H_2O ordering and superstructures in armenite, $BaCa_2Al_6Si_9O_{30}\cdot 2H_2O$: A single-crystal X-ray and TEM study

THOMAS ARMBRUSTER
Laboratorium für chemische und mineralogische Kristallographie, Universität Bern, Freiestr. 3, CH-3012 Bern, Switzerland
MICHAEL CZANK
Mineralogisch-petrographisches Institut und Museum, Universität Kiel, Olshausenstr. 40, D-2300 Kiel, Germany

ABSTRACT

Optical microscopy, transmission electron microscopy, and X-ray diffraction were used to study armenite samples from the Armen mine, Norway; from Rémigny, Quebec, Canada; and from Wasenalp, Vallis, Switzerland. All armenite samples studied can be described as cyclic twins of orthorhombic domains leading to pseudohexagonal morphology. Electron and X-ray diffraction patterns indicate various types of orthorhombic superstructures. The crystal structures of samples from Rémigny and the Armen mine were refined from single-crystal X-ray data in the space group *Pnna* with $a = 13.874(2)$, $b = 18.660(2)$, $c = 10.697(1)$ Å, $Z = 4$. The structure belongs to the double-ring silicate type but deviates from hexagonal symmetry. This deviation occurs for two reasons: (1) H_2O is ordered on B′ sites, which causes the lattice to be primitive orthorhombic, and Ca is sevenfold coordinated by six O atoms of the tetrahedral framework and one H_2O; (2) partial (Si,Al) ordering reduces the symmetry to orthorhombic. The *Pnna* structural model exhibits some completely (Si,Al)-ordered tetrahedra and additional tetrahedral sites for which T-O distances indicate an Si/Al ratio of 1.

INTRODUCTION

Neumann (1939) first recognized armenite as a new mineral when he reanalyzed a sample from the Armen mine in Norway. Neumann (1941) grouped armenite as a milarite-related, biaxial (orthorhombic?) silicate of optic negative character, $2V_x = 60°$, and with the composition of $BaCa_2Al_6Si_9O_{30}\cdot 2H_2O$. Armenite is pseudohexagonal and forms penetration twins of domains related by an angle of 120° (Neumann, 1941). Bakakin et al. (1975) performed X-ray single-crystal structure studies of double-ring silicates including armenite from the Norwegian locality. These authors were aware of the twinning but refined an average structure of a pseudohexagonal twin in space group *P6/mcc* as known for other double-ring silicates. Armenite has erroneously been considered to be hexagonal since that study. A second occurrence was described from Rémigny, Quebec, Canada, where armenite forms veins together with albite, manganoan zoisite ("thulite"), and piedmontite (Pouliot et al., 1984). Mason (1987) reports that the mineral calciocelsian found in the Ba-rich aplitic gneisses at Broken Hill is actually armenite. Armenite was also described by Semenenko et al. (1987), Žák and Obst (1989), Balassone et al. (1989), and Fortey et al. (1991). Recently, armenite was collected (Senn, 1990) as an alpine fissure mineral from the celsian-bearing leucocratic gneisses of the Simplon area, Lepontine Alps in Switzerland (Frank, 1979).

In a previous study of milarite, a closely related double-ring silicate with the formula $KNa_{1-x}Ca_2(Be_{3-x}Al_x)Si_{12}O_{30}[nH_2O]$, it was suggested (Armbruster et al., 1989) that optical sectors resembling a trilling pattern in (001) sections are caused by variable ordering of H_2O. Nonstoichiometric H_2O increases the O coordination of Ca from six to seven.

Armbruster (1988) relates the optical sectors in armenite to (Si,Al) ordering. It may be assumed that with respect to (Si,Al) ordering and the high Al/Si ratio, armenite is the double-ring analogue to cordierite, $(Mg,Fe)_2Al_4Si_5O_{18}$, which has a single six-membered ring. Cordierite occurs in two modifications, low cordierite and high cordierite or indialite. The first is a completely (Si,Al)-ordered orthorhombic modification (e.g., Cohen et al., 1977; Putnis et al., 1985), and the second is a hexagonal (Si,Al)-disordered modification (Meagher and Gibbs, 1977; Armbruster, 1985).

Pouliot et al. (1984) and Žák and Obst (1989) describe biaxial and uniaxial armenite domains within one-crystal aggregate. Heat treatment of armenite for 4 d at 950 °C (Pouliot et al., 1984) or 1000 °C (Balassone et al., 1989) causes expulsion of the H_2O and leads to uniaxial optical properties with decreased refractive indices. After heating, the twinning pattern disappears and the cell volume is reduced. These experiments seem to indicate that the observed sectoring in natural armenite may be related to

0003–004X/92/0304–0422$02.00

the presence of H_2O. The present study was performed to analyze the influence of H_2O and (Si,Al) ordering on the structure of armenite and its optical properties.

Experimental methods

Electron microscopy

For transmission electron microscopy (TEM) studies, crystal grains from Rémigny, Quebec, Canada, and from Wasenalp, Vallis, Switzerland, were used. The samples were ground, suspended in ethanol (99.9%), and deposited on holey carbon films. The TEM investigations were performed with a Philips EM 400T operated at 100 kV. A rotation-tilt specimen holder (360° and ±60°) was used for diffraction studies and high resolution imaging. For the latter, care was taken to insure the critical alignment and experimental conditions as described by Buseck and Iijima (1974).

X-ray diffraction

Precession (Mo$K\alpha$) and Weissenberg (Fe$K\alpha$) diffraction patterns of optically twinned aggregates of armenite from Canada, Norway, and Switzerland were recorded in various orientations. Guinier powder photographs (Fe$K\alpha_1$ radiation) of the Canadian armenite sample were taken before and after heating 72 h at 1000 °C.

Single-crystal separation

A rock sample of the Canadian armenite was available, and an uncovered thin section (75 μm thick) of intergrown twin aggregates was prepared parallel to (001). Two optically homogeneous areas were selected and drilled out with the microdrilling device of Medenbach (1986). Two disks with a diameter of 200 μm were obtained. Because only small twins of the Norwegian armenite were available, one twin was crushed and the fragments were optically tested for homogeneity with a polarizing microscope equipped with a spindle stage. An irregularly shaped fragment of 50 × 100 × 150 μm was selected for further investigations.

Single-crystal data measurement and structure refinement

A Canadian crystal with fairly sharp superstructure reflections and the Norwegian crystal were used for data measurement at room temperature using an Enraf Nonius CAD4 diffractometer with graphite monochromated Mo$K\alpha$ X-radiation. Previous electron microprobe analyses showed no significant deviation from end-member stoichiometry for all samples. A 2.5° ω scan in combination with a 2.5-mm horizontal aperture were selected to obtain reliable X-ray intensities, including streaked reflections. Table 1 gives additional details. Reflections in one octant of reciprocal space were obtained up to θ = 30° without assuming any absences. An empirical absorption correction was applied using the ψ scan technique. Data reduction, including background and Lorentz-polarization corrections, was performed with the SDP program system (Enraf Nonius, 1983). Starting values for the refinement were obtained by direct methods with the program SHELXS-86 (Sheldrick, 1986) and subsequent difference-Fourier analyses. Reflections allowed for space group *Pnna* with $F_{obs} > 6\sigma(F_{obs})$ and unit weights were used for refinement with the program SHELX76 (Sheldrick, 1976). Neutral-atom scattering factors and real as well as imaginary anomalous dispersion corrections were applied. Assignment of Si,Al scattering factors to the tetrahedral positions (T) was done on the basis of T-O distances obtained in test cycles. To avoid correlation problems and to maintain a ratio of approximately 10:1 between observations and refined parameters, anisotropic displacement amplitudes were only refined for Ba, Ca, and H_2O. Final difference-Fourier maps showed residual densities up to 1 electron/Å^3 in the neighborhood of (Si,Al) sites and −2 electrons/Å^3 close to Ba. The fairly low quality of the refinement is probably caused by the diffuse character of the superstructure reflections and the platy shape of the crystal fragment, making the absorption correction imprecise.

Table 1. Experimental details of data measurement and structure refinement of armenite from Rémigny, Quebec, Canada

Space group	*Pnna*
Cell dimensions a = 13.874(2), b = 18.660(2), c = 10.697(1) Å (from Guinier photographs)	
Upper θ limit	30°
Scan type	ω 2.5°
No. of measured reflections	4500
No. of unique reflections	3165
No. of reflections with $F_{obs} > 6\sigma(F_{obs})$	1510
Absorption correction	applied
Anomalous dispers. correction	applied
No. of refined parameters	115
R (%)	5.1
R_w (%)	5.6

Note: $R = \Sigma \| |F_{obs}| - |F_{calc}| \| / \Sigma |F_{obs}|$, $R_w = (\Sigma w(|F_{obs}| - |F_{calc}|)^2 / \Sigma w|F_{obs}|^2)^{1/2}$.

By analogy with other double-ring silicates (e.g., Armbruster et al., 1989) the following nomenclature was used. T2 refers to ring-forming tetrahedra and T1 refers to ring-connecting tetrahedra. The second numbers (e.g., T11, T21) are arbitrarily chosen to label corresponding sites. O1-type O atoms link six-membered rings to double rings, O2-type O atoms connect tetrahedra to form rings, and O3 sites link the ring-connecting tetrahedra (T1) to the double-ring units. Observed and calculated structure factors are given in Table 2.[1]

Results

Armenite samples from Rémigny and the Armen mine yielded very similar diffraction results, whereas the Wasenalp sample behaved significantly differently.

[1] To obtain a copy of Table 2, order Document AM-92-492 from the Business Office, Mineralogical Society of America, 1130 Seventeenth Street NW, Suite 330, Washington, DC 20036, U.S.A. Please remit $5.00 in advance for the microfiche.

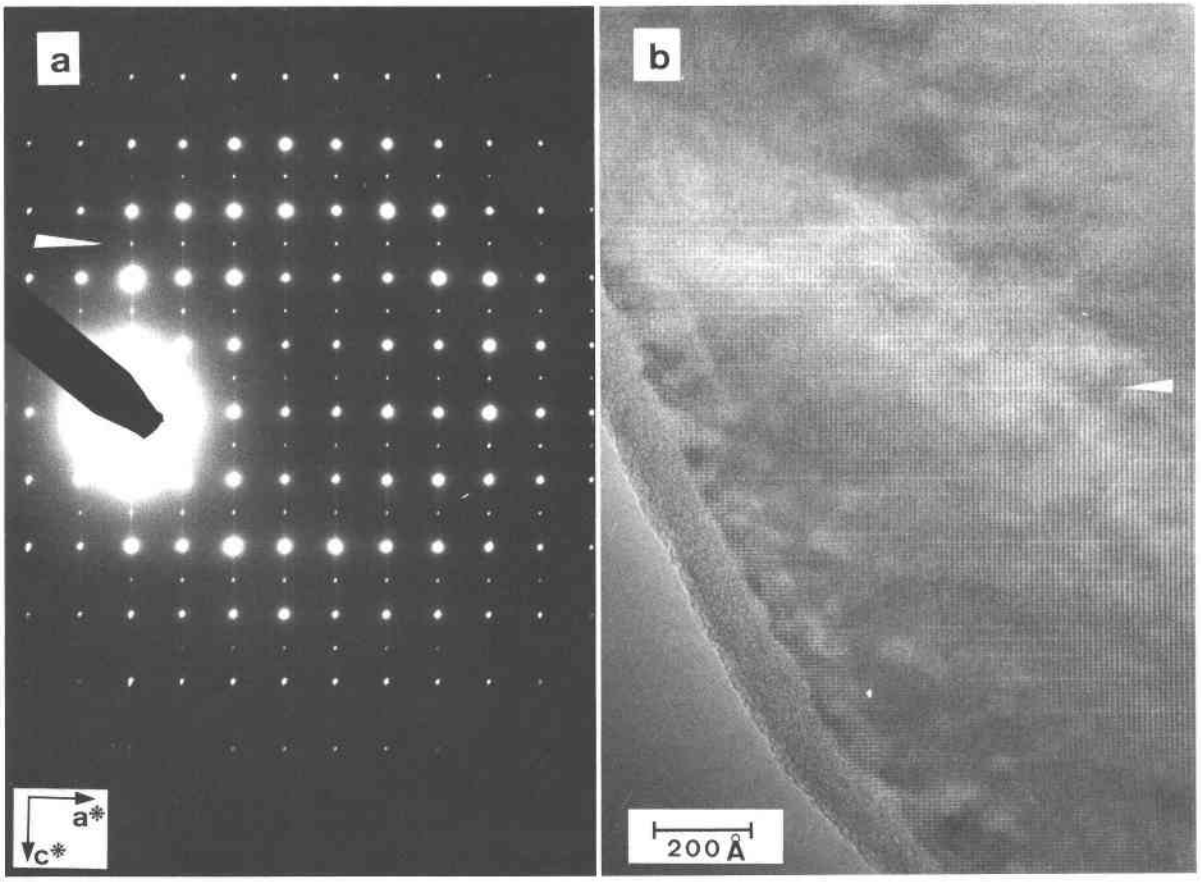

Fig. 1. (**a**) Electron diffraction pattern of armenite from Rémigny, Quebec, Canada. The **a***-**c*** (hexagonal-indexed) pattern shows diffuse streaks along **c*** with additional reflections of the type $h0l$ with $l = 2n + 1$ (marked by white arrow), which are forbidden in space group $P6/mcc$. (**b**) High magnification TEM structure image of a crystal from Rémigny, Quebec, Canada, with the same orientation (hexagonal-indexed) as in **a**. Numerous dislocations perpendicular to the **c** axis were interpreted as faults probably related to H_2O defects.

Rémigny and Armen mine samples

All Rémigny crystals studied by TEM gave equivalent results. A hexagonal-indexed **a***-**c*** electron diffraction pattern (Fig. 1a) shows diffuse streaks along **c*** and reflections of the type $h0l$ with $l = 2n + 1$ (forbidden in space group $P6/mcc$). The corresponding structure image (Fig. 1b) exhibits numerous zipperlike dislocations parallel to (001), which were interpreted as faults caused by H_2O defects and probably related to the streaking along **c*** in the electron diffraction patterns. An $\mathbf{a}_1$*-$\mathbf{a}_2$* diffraction pattern shows no deviation from hexagonal symmetry. After focusing the electron beam for high-resolution imaging, superstructure reflections were not present in subsequent electron diffraction photographs.

The $hk0$ and $hk1$ X-ray precession photographs of optically twinned crystals are consistent with space group $P6/mcc$ or $P62cc$ and give cell dimensions $a \approx 10.7$ Å, $c \approx 13.9$ Å, but $hk2$ photographs (Fig. 2a) clearly show additional reflections inconsistent with the hexagonal model. The X-ray pattern can be interpreted as being caused by cyclic twinning of primitive orthorhombic domains with $a \approx 18.7$, $b \approx 10.7$, $c \approx 13.9$ Å.

The single crystals (two from Canada and one from Norway) separated from twins showed slightly undulatory extinction under the polarizing microscope. The optic axial angle (at 589 nm) refined from spindle stage extinction data (Bloss, 1981) varied between $2V_x = 59$ and 60°. Subsequent $hk2$ precession photographs confirmed the primitive orthorhombic lattice for armenite (Fig. 2b). Reflections that violate a face-centered lattice are more diffuse and slightly smeared out along **a***. This streaking varies from crystal to crystal. Systematic extinctions suggest space group $Pnna$. In the $Pnna$ standard setting, the unit-cell axes are transformed to $a \approx 13.9$, $b \approx 18.7$, $c \approx 10.7$ Å.

In agreement with the single-crystal results, an X-ray powder pattern of the unheated sample from Rémigny showed several split reflections (Žák and Obst, 1989) and could only be indexed using an orthorhombic lattice. The orthorhombic cell dimensions refined (space group $Pnna$) to the values $a = 13.874(2)$, $b = 18.660(2)$, $c = 10.697(1)$

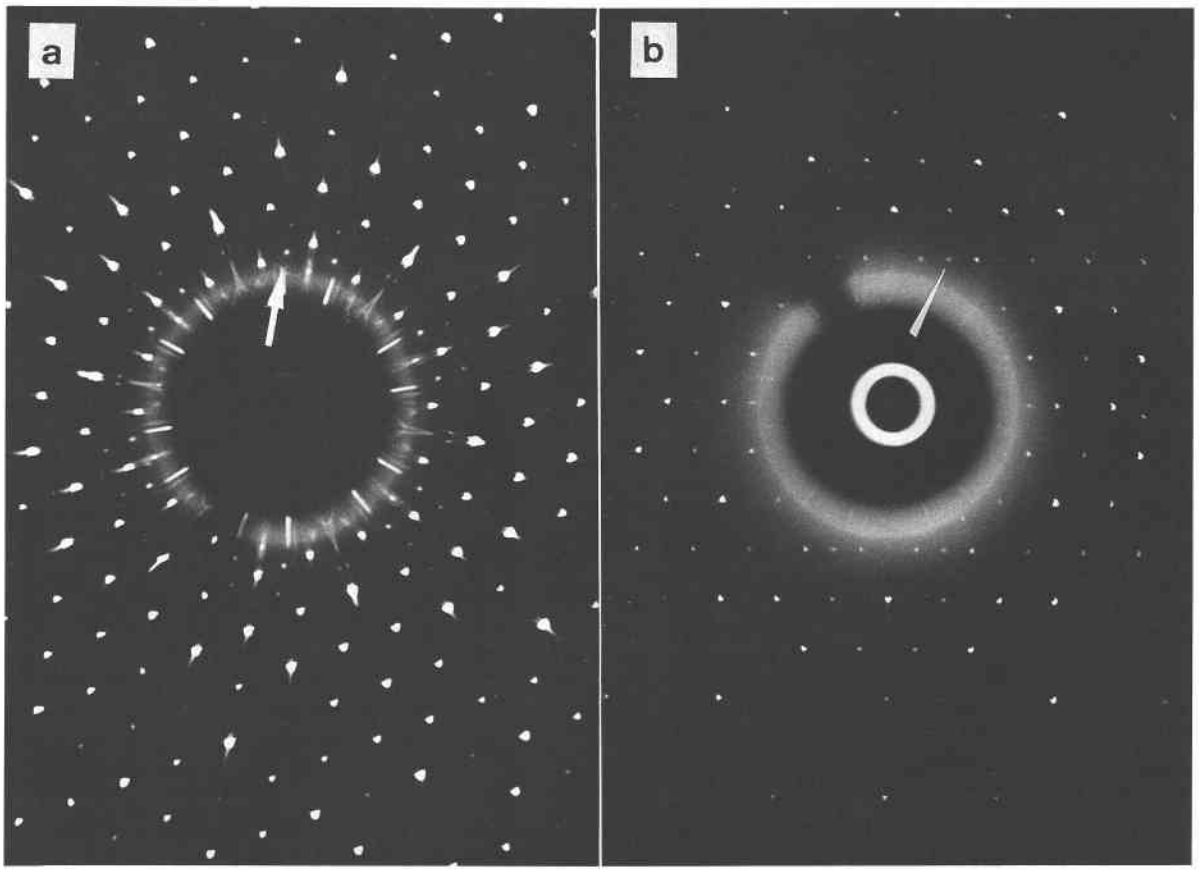

Fig. 2. (**a**) Strongly overexposed precession photograph [*hk*2 layer in pseudohexagonal setting ($c \approx 13.9$ Å)] of a cyclic twinned crystal from Rémigny, Quebec, Canada. Superstructure reflections (white arrow) of twinned domains show a primitive orthorhombic lattice. (**b**) Precession photograph [*hk*2 layer in pseudohexagonal setting ($c \approx 13.9$ Å)] of a separated single crystal from the Armen mine, Norway, showing fairly sharp superstructure reflections. The photograph shows obvious deviation from hexagonal symmetry. In *Pnna* setting the photograph represents a 2*hk* layer.

Å. The splitting was not present after heat treatment (72 h at 1000 °C), and the pattern could be indexed with a hexagonal cell with parameters $a = 10.614(1)$, $c = 14.020(5)$ Å.

Structure refinements of crystals from Canada and Norway yielded similar results, but because of the larger size of the Canadian crystal more observable reflections could be measured. Thus only the results for the Canadian armenite are presented. Fractional coordinates are given in Table 3; interatomic distances and angles are summarized in Table 4. Two structural features account for the deviation from hexagonal symmetry: (1) The O position of the H_2O molecule is incompatible with hexagonal symmetry and increases coordination of a CaO_6 octahedron to sevenfold. (2) Out of nine tetrahedral sites, two (T21 and T26) have T-O distances (Table 4) characteristic of Si occupancy with d(Si-O) = 1.62 Å and one (T11) characteristic of Al occupancy with d(Al-O) = 1.74 Å. The remaining six sites display T-O distances [d(Si,Al)-O $\approx$ 1.68 Å] characteristic of an Si/Al ratio of 1/1. Figure 3 shows a projection of the double-ring structure along **a** with H_2O molecules (drawn as circles) lying above the corresponding CaO_6 octahedra with d[Ca-O(H_2O)] = 2.44 Å. In cases where the H_2O molecule is not shown, it is below the CaO_6 octahedra. The H_2O arrangement leads to undulating chains of Ca octahedra sharing edges with Si/Al = 1 tetrahedra parallel to the **c** axis (10.7 Å). Within these chains the H_2O molecule occurs either above or below the CaO_6 unit. Chains with H_2O above the octahedra alternate with chains where H_2O is below the octahedra. The Al tetrahedron T11 shares edges with one Ca octahedron with H_2O above and one with H_2O below and connects the chains to rings. (Si,Al) disorder is observed for those tetrahedra that link CaO_6 units with the H_2O molecule positioned at the same height along **a** when considering the 12-membered rings of edge-sharing octahedra and tetrahedra. Thus there seems to be a correlation between the H_2O arrangement and (Si,Al) order-disorder. Ba occupies the C site and is 12-coordinated with an average Ba-O distance of 3.01 Å.

TABLE 3A. Atomic positional parameters and B_{eq} values for armenite from Canada

Atom	x	y	z	B_{eq} (Å²)
C(Ba)	¼	0	0.0052(2)	1.15(2)
A(Ca)	0.2714(2)	−0.1679(1)	−0.4990(4)	1.17(4)
T11(Al)	¾	0	0.4977(9)	0.78(6)*
T12(Si,Al)	0.2461(4)	¾	¾	0.6(2)*
T13(Si,Al)	0.2456(5)	¾	¼	1.0(2)*
T21(Si)	0.1161(4)	−0.0435(3)	−0.2914(4)	0.77(7)*
T22(Si,Al)	0.3879(4)	0.1237(2)	0.2113(4)	0.80(8)*
T23(Si,Al)	0.3826(4)	−0.1209(2)	−0.2052(4)	0.84(8)*
T24(Si,Al)	0.1137(3)	−0.1655(3)	−0.0802(4)	0.71(6)*
T25(Si,Al)	0.1149(3)	0.1630(3)	0.0859(4)	0.81(6)*
T26(Si)	0.6104(4)	0.0404(3)	0.7050(4)	0.77(7)*
B'(H_2O)	−0.0523(7)	−0.1748(6)	−0.507(1)	2.5(2)
O31	0.3134(8)	−0.2678(6)	−0.623(1)	1.0(2)*
O32	0.3131(7)	−0.1779(6)	−0.288(1)	0.9(2)*
O33	0.1823(8)	−0.0618(6)	−0.413(1)	0.7(2)*
O34	0.1813(8)	−0.2620(6)	−0.381(1)	0.9(2)*
O35	0.1790(7)	−0.1795(6)	−0.699(1)	1.1(2)*
O36	0.3257(8)	−0.0570(7)	−0.582(1)	1.1(2)*
O21	0.137(1)	−0.0988(8)	−0.180(1)	2.1(3)*
O22	0.3588(8)	0.1337(6)	0.061(1)	1.3(2)*
O23	0.3571(9)	−0.1264(6)	−0.052(1)	1.7(2)*
O24	0.138(1)	0.0955(8)	0.184(1)	2.0(3)*
O25	0.360(1)	0.0376(8)	0.243(1)	2.1(2)*
O26	0.8554(9)	−0.0347(7)	0.238(1)	1.4(2)*
O11	0.003(1)	0.1396(4)	0.7588(8)	1.3(1)*
O12	0.502(1)	0.9557(4)	0.3300(7)	1.3(1)*
O13	0.501(1)	0.3097(4)	0.5873(7)	1.2(1)*

Note: $B_{eq} = {}^8/_3\,\pi^2\Sigma_i[\Sigma_j(U_{ij}a_i^*a_j^*a_ia_j)]$; $\sigma(B_{eq})$: Schomaker and Marsh (1983).
* Atoms refined isotropically.

TABLE 3B. Anisotropic displacement parameters (× 10²)

Atom	U_{11}	U_{22}	U_{33}	U_{12}	U_{13}	U_{23}
Ba	2.33(5)	1.05(4)	1.00(5)	0.07(6)	0	0
Ca	2.51(4)	1.01(9)	0.92(8)	−0.14(9)	−0.0(2)	0.0(2)
H_2O	2.4(5)	3.7(6)	3.7(6)	0.1(5)	0.3(6)	2.2(7)

Note: Displacement parameters are of the form $\exp[-2\pi^2(U_{11}h^2a^{*2} + U_{22}k^2b^{*2} + U_{33}l^2c^{*2} + 2U_{12}hka^*b^* + 2U_{13}hla^*c^* + 2U_{23}klb^*c^*)]$.

Wasenalp, Vallis, sample

Different electron diffraction patterns were observed in hexagonal-indexed **a***-**c*** photographs of various grains. These patterns are classified into three types. Type a: The diffraction pattern shows strong reflections of the type $h0l$ with $l = 2n + 1$ (Fig. 4a). Diffuse streaks along **c*** of the kind observed for the Rémigny sample were not observed. Type b: Figure 4b shows the diffraction pattern that exhibits only weak reflections of the type $h0l$ with $l = 2n + 1$. Superstructure reflections connected by diffuse streaks are observed at ⅓ and ⅔ along **a***. Type c: This type differs from the other two types because reflections of the type $h0l$ with $l = 2n + 1$ and diffuse streaks are not observed, but superstructure reflections occur at ½ along **a*** but not at ⅓ and ⅔ along **a***. Diffuse streaks are also missing. Corresponding structure images of all types appear homogeneous and show only low concentrations

TABLE 4. Selected interatomic distances (Å) and angles (°) for armenite

Ba-O21 2×	3.13	Ca-O(H_2O)	2.45		
-O22 2×	2.98	-O32	2.34		
-O23 2×	2.85	-O33	2.51		
-O24 2×	3.04	-O35	2.50		
-O25 2×	3.05	-O36	2.38		
-O26 2×	3.05	-O31	2.36		
		-O34	2.49		
T11-O33 2×	1.74	T12-O32 2×	1.68	T13-O31 2×	1.69
-O36 2×	1.75	-O34 2×	1.68	-O35 2×	1.70
O33-T11-O36	110.4	O32-T12-O34	112.8	O31-T13-O35	114.1
O33-T11-O36	101.1	O32-T12-O32	113.0	O31-T13-O31	112.2
O33-T11-O33	117.2	O32-T12-O34	101.8	O31-T13-O35	101.5
O36-T11-O36	117.6	O34-T12-O34	115.1	O35-T13-O35	114.0
T21-O33	1.63	T22-O35	1.69	T23-O32	1.68
-O21	1.60	-O22	1.67	-O23	1.68
-O12	1.63	-O25	1.68	-O26	1.69
-O26	1.62	-O11	1.66	-O11	1.67
O33-T21-O21	110.7	O35-T22-O22	110.1	O32-T23-O23	110.5
O33-T21-O12	110.0	O35-T22-O25	110.5	O32-T23-O26	111.5
O33-T21-O26	109.6	O35-T22-O11	108.1	O32-T23-O11	106.9
O21-T21-O12	111.1	O22-T22-O25	104.1	O23-T23-O26	102.2
O21-T21-O26	105.9	O22-T22-O11	113.6	O23-T23-O11	114.4
O12-T21-O26	109.6	O25-T22-O11	110.5	O26-T23-O11	111.4
T24-O34	1.70	T25-O31	1.68	T26-O36	1.61
-O21	1.68	-O23	1.68	-O24	1.62
-O13	1.66	-O24	1.67	-O25	1.61
-O22	1.67	-O13	1.66	-O12	1.61
O34-T21-O21	109.0	O31-T25-O23	112.6	O36-T26-O24	110.3
O34-T24-O13	107.3	O31-T25-O24	108.8	O36-T26-O25	108.6
O34-T24-O22	112.4	O31-T25-O13	109.1	O36-T26-O12	109.7
O21-T24-O13	111.5	O23-T25-O24	101.7	O24-T26-O25	105.0
O21-T24-O22	105.7	O23-T25-O13	110.7	O24-T26-O12	111.7
O13-T24-O22	111.1	O24-T25-O13	114.0	O25-T26-O12	111.5
T22-O11-T23	146.6	T21-O12-T26	151.7	T24-O13-T25	145.8
T21-O21-T24	156.6	T22-O22-T24	149.1	T23-O23-T25	146.9
T25-O24-T26	153.8	T22-O25-T26	150.9	T23-O26-T21	151.4
T13-O31-T25	132.2	T12-O32-T23	134.1	T11-O33-T21	125.6
T12-O34-T24	127.5	T13-O35-T22	126.6	T11-O36-T26	129.4

Note: Estimated standard deviations of distances are 0.01 Å and 0.7° for angles.

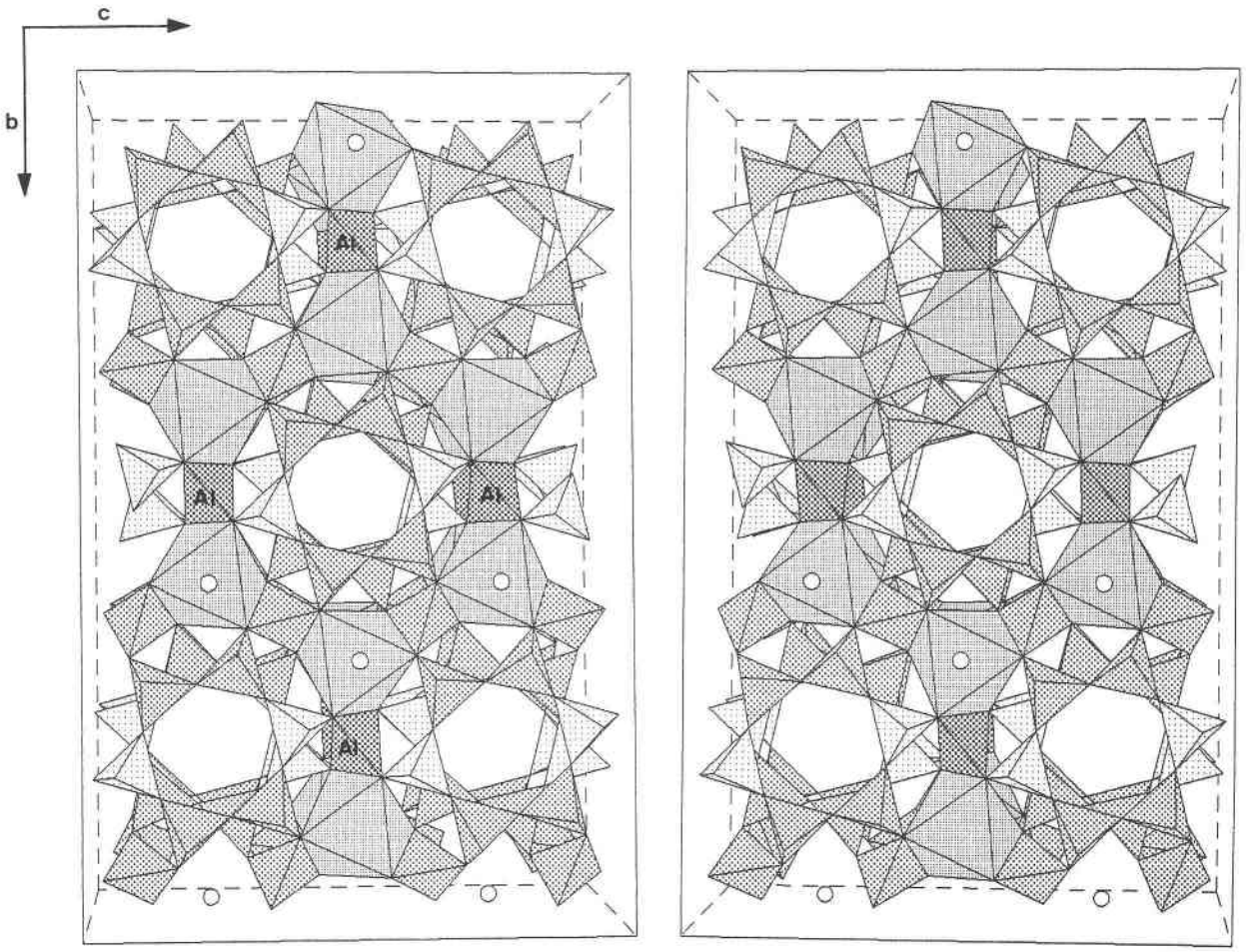

Fig. 3. Stereoscopic diagram of partially (Si,Al)-ordered armenite in space group *Pnna*, projected along the channel axis (**a** axis in this setting). This (Si,Al) distribution is consistent with a face-centered lattice. H_2O molecules (open spheres) above or below the CaO_6 octahedra lead to symmetry reduction. Si tetrahedra are shown with a light dotted pattern, Al tetrahedra are shown with a dark dotted pattern, and Si/Al = 1/1 tetrahedra are intermediate. Ba between the 12-membered double rings is not shown.

of dislocations. No additional reflections are observed in $\mathbf{a}_1^*$-$\mathbf{a}_2^*$ diffraction patterns.

As in the case of the Rémigny and Armen mine samples, *hk*0 and *hk*1 (hexagonal-indexed) X-ray precession photographs are in agreement with space group *P*6/*mcc* or *P*62*c*. The *hk*2 photographs (Fig. 5) were also interpreted as being caused by cyclic twinning of an orthorhombic lattice about the pseudo-sixfold axis. In addition, the orthorhombic lattice has a superstructure with six times the repeat distance of the basis structure along **a**. Reflections at $\mathbf{a}^* = \frac{1}{3}$ and $\frac{2}{3}$ are streaked along $\mathbf{a}^*$. Different fragments of the same twin aggregate of the Wasenalp sample exhibit mixtures of the Canadian-Norwegian domain type and the type only observed for the Swiss armenite sample (reflections at $\frac{1}{3}$ and $\frac{2}{3}$ along $\mathbf{a}^*$).

Discussion

H_2O arrangement

All observed superstructure reflections that are incompatible with an orthorhombic face-centered lattice are caused by the arrangement of the H_2O molecules. Even a perfectly (Si,Al)-ordered [according to the Loewenstein (1954) rule] anhydrous armenite sample can be described with a face-centered orthorhombic lattice. Thus the observed streaking of the superstructure reflections, which varies from crystal to crystal, indicates slight H_2O disorder. This disorder might also be related to the dislocations observed in high-magnification TEM structure images. The different type of superstructure reflections found in some armenite samples (Vallis) probably indicates different H_2O arrangements. The observation that superstructure reflections are not present after focusing the electron beam for high-resolution imaging emphasizes the sensitivity of the H_2O orientation and suggests that the electron beam has sufficient energy to disorder or expel H_2O. H_2O release is not required in order to explain the loss of the superstructure reflections. The H_2O can move within the B site from $x \approx -0.05$ to $x \approx 0.05$ (or vice versa) and thus disturb the ordering pattern. Two explanations can be given: (1) Within a stack parallel to

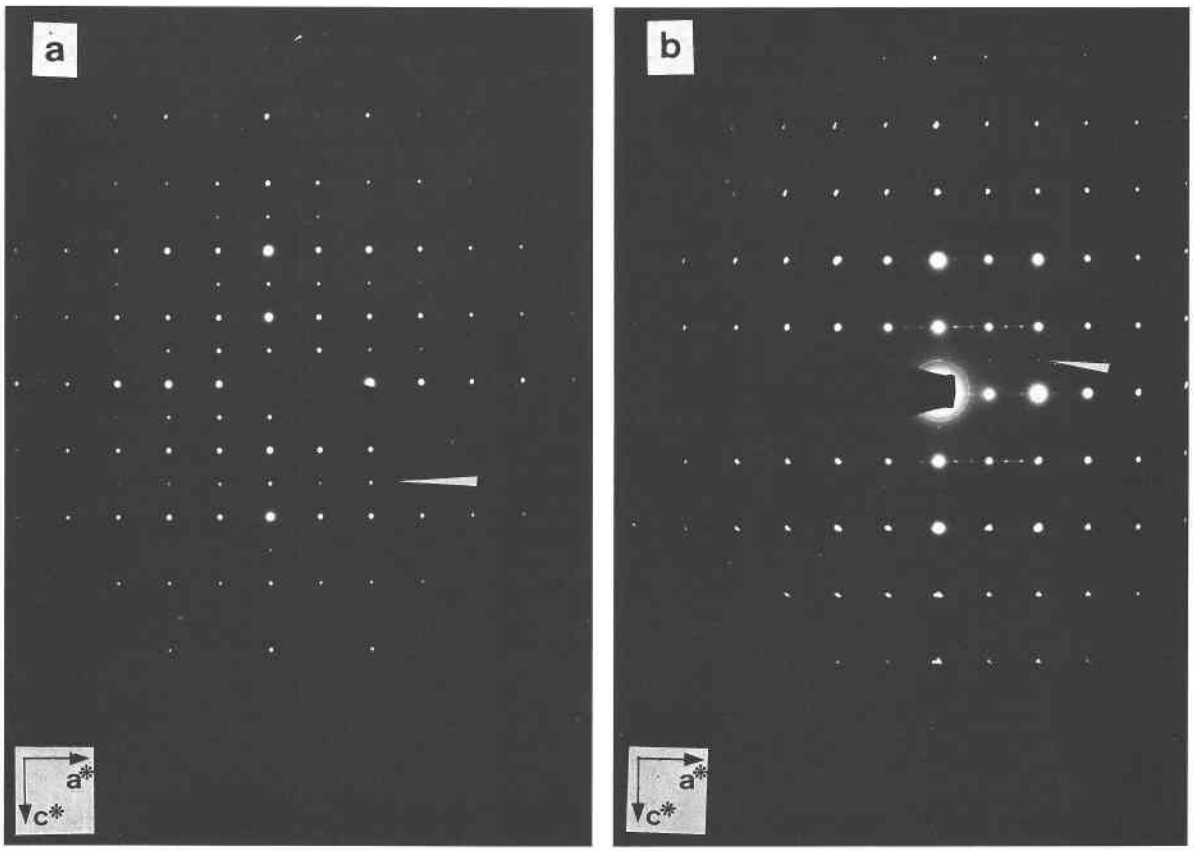

Fig. 4. (**a**) Electron diffraction pattern of armenite from Wasenalp, Vallis, Switzerland. The **a***-**c*** (hexagonal-indexed) pattern was classified as type a and shows strong reflections (marked by white arrow) of the type $h0l$ with $l = 2n + 1$ (forbidden in space group $P6/mcc$). No diffuse streaks are observed when comparing this pattern with Figure 1a. (**b**) Electron diffraction pattern of armenite from Wasenalp, Vallis, Switzerland. The **a***-**c*** (hexagonal-indexed) pattern was classified as type b and shows weak reflections of the type $h0l$ with $l = 2n + 1$ (marked by white arrow). In addition, superstructure reflections occur at $\frac{1}{3}$ and $\frac{2}{3}$ along **a*** connected by diffuse streaks.

a, each H_2O changes to the opposite B′ site and Ca remains seven-coordinated. (2) If H_2O vacancies exist within one stack, the position of the H_2O molecule may change at the vacancy from up to down. If H_2O disorder occurs in the absence of vacancies, some Ca will be eight- and some six-coordinated.

A similar behavior was observed for the structurally related milarite $KNa_{1-x}Ca_2(Be_{3-x}Al_x)Si_{12}O_{30}[nH_2O]$, which contains nonstoichiometric H_2O. This mineral is described in space group $P6/mcc$ but exhibits unusual biaxial sectors in (001) sections (e.g., Janeczek, 1986; Armbruster et al., 1989). These sectors were explained by symmetry reduction owing to ordering of H_2O molecules that may occupy a position above or below a CaO_6 octahedron. Superstructure reflections were not observed for milarite. As already postulated for milarite (Armbruster et al., 1989), Ca in armenite is seven-coordinated and exhibits distances to the six O atoms that are approximately equal and that form a distorted octahedron with an additional H_2O molecule.

(Si,Al) ordering

With the observed H_2O arrangement, a hypothetical, fully ordered armenite sample (Fig. 6) would crystallize in acentric space group $Pnc2$ ($a \approx 18.7$, $b \approx 10.7$, $c \approx 13.9$ Å) and give different systematic extinctions compared with those of the observed space group $Pncn$ ($Pnna$ in standard setting). Intensities of reflections defining the difference between the two space groups were carefully measured, and only one reflection (indices 13,2,0) was found to have weak but significant intensity, $F_{obs} = 12\sigma(F_{obs})$. A subsequent test refinement in $Pnc2$ did not converge because of correlation problems. Introduction of bond-length constraints, which predefine the assumed (Si,Al) distribution according to Loewenstein's (1954) rule, did not lead to an improvement of the agreement factor compared with the $Pncn$ refinement. Thus the X-ray diffraction experiments cannot resolve whether armenite is only partially or fully ordered. In the authors' view and experience with cordierite and feldspars, it appears very

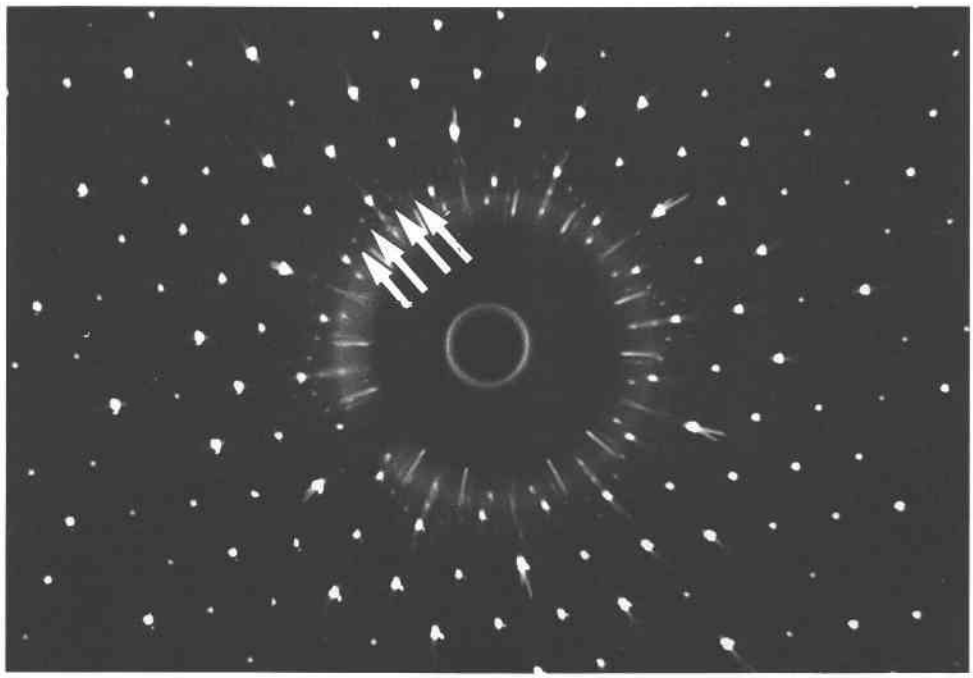

Fig. 5. Strongly overexposed precession photograph (*hk*2 layer in pseudohexagonal setting; $c \approx 13.9$ Å) of a cyclic twinned crystal from Vallis, Switzerland. Superstructure reflections are observed at ⅓ and ⅔ along **a*** (marked by white arrows) in addition to the weak reflections seen in Figure 2a.

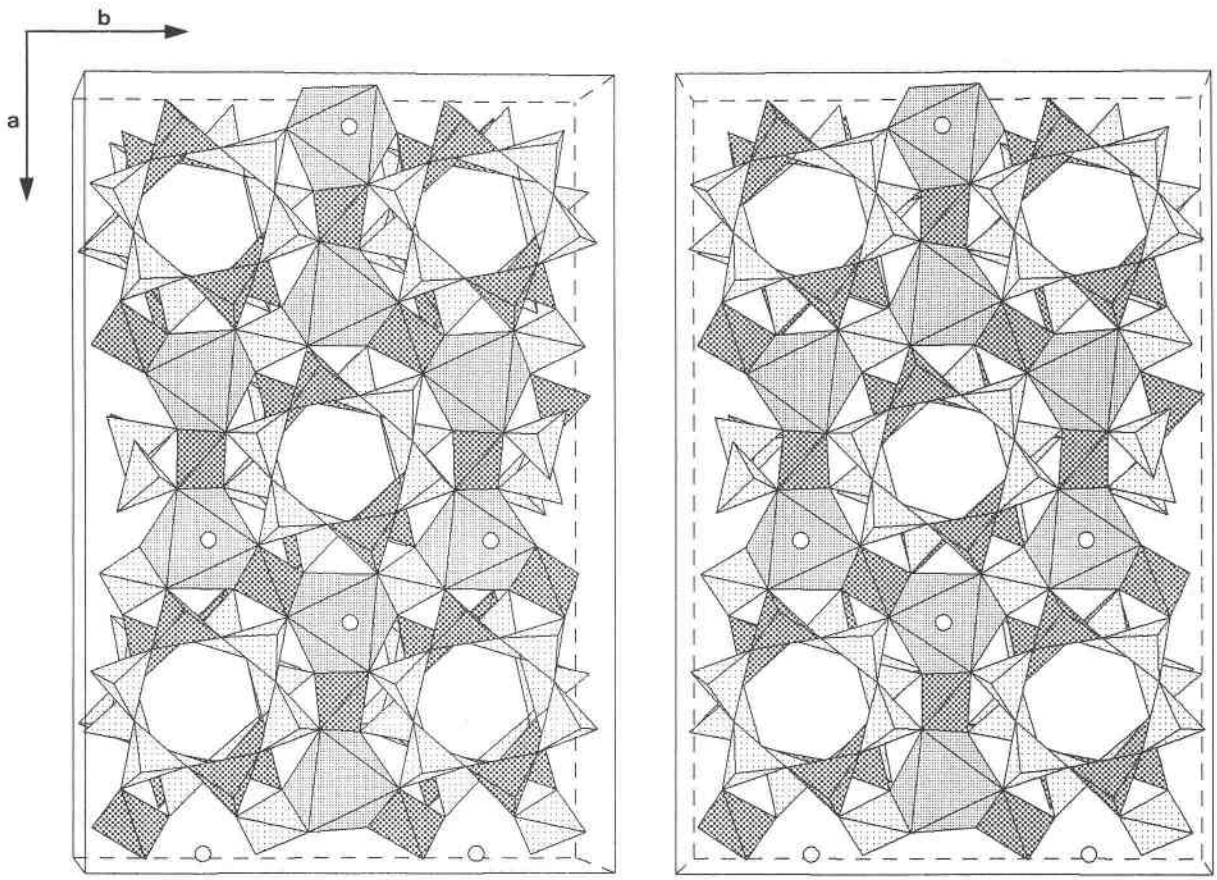

Fig. 6. Stereoscopic diagram of armenite completely (Si,Al)-ordered in space group *Pnc*2 ($a \approx 18.7$, $b \approx 10.7$, $c \approx 13.9$ Å), projected along the channel axis (**c** axis in this setting). The (Si,Al) distribution is consistent with a face-centered lattice. H_2O molecules (open spheres) above or below the CaO_6 octahedra lead to symmetry reduction. Si tetrahedra shown with a light dotted pattern, Al tetrahedra are indicated by a dark dotted pattern. Ba between the 12-membered double rings is not shown.

unusual that within one structure some positions reveal complete (Si,Al) ordering (T11, T21, T26), whereas other sites show an Si/Al ratio of 1/1 (T12, T13, T22, T23, T24, T25). It could be argued that additional submicroscopic twinning is responsible for the observed (Si,Al)-disordered positions. However, TEM studies (Rémigny sample) do not support this hypothesis, and single-crystal X-ray experiments (Armen mine and Rémigny samples) show only reflections compatible with space group *Pnna*. A final decision about short-range (Si,Al) ordering in armenite must await a solid-state MAS ^{29}Si NMR study currently in progress.

Behavior upon heating

Previous heating experiments by Neumann (1941), Pouliot et al. (1984), and Balassone et al. (1989) showed that upon heating to ca. 1000 °C, H_2O is expelled from armenite. Our experiments on armenite single crystals that were heated for 72 h at 1000 °C indicated that the superstructure reflections (characteristic of the primitive lattice) became unobservable and the crystal became metrically hexagonal. However, based on (Si,Al) order-disorder relations in cordierite (e.g., Schreyer, 1966), it is not likely that these fairly moderate conditions are sufficient to cause complete (Si,Al) disorder within T1 and T2 tetrahedra. Thus, armenite heated under these conditions is probably only pseudohexagonal and possesses the same (Si,Al) arrangement as natural armenite. The corresponding space group symmetry is *Amma* (in a setting corresponding to *Pnna*; standard setting is *Cccm*).

Heating also leads to a significantly smaller molar volume [heated: 2735.7(4) Å^3, natural: 2769.3(4) Å^3], whereas the length of the channel axis shows opposite behavior. A corresponding behavior has been observed for the dehydration of milarite (Armbruster et al., 1989) that is related to distortions of the Ca coordination (sevenfold coordination in the natural sample vs. distorted octahedral distortion in the dehydrated crystal).

Acknowledgments

The armenite sample from Rémigny, Canada, was obtained from H.A. Stalder (Naturhistorisches Museum Bern, sample NMBE-B4468), armenite from Wasenalp was donated by S. Graeser (Naturhistorisches Museum Basel), and armenite from the type locality in Norway was received from the Mineralogisk-Geologisk Museum of Oslo University, all of which are highly appreciated. M. Kunz and Vladimir Malogajski are thanked for their assistance. We are indebted to John Chermak for improving the English.

References cited

Armbruster, Th. (1985) Crystal structure refinement, Si,Al-ordering, and twinning in "pseudo-hexagonal" Mg-cordierite. Neues Jahrbuch für Mineralogie Monatshefte, 1985, 255–267.

——— (1988) Relations between structure, chemistry and optical properties: Applications in mineralogy. Zeitschrift für Kristallographie, 185, 107.

Armbruster, Th., Bermanec, V., Wenger, M., and Oberhänsli, R. (1989) Crystal chemistry of double-ring silicates: Structure of natural and dehydrated milarite at 100 K. European Journal of Mineralogy, 1, 353–362.

Bakakin, V.V., Balko, V.P., and Solov'eva, L.P. (1975) Crystal structures of milarite, armenite, and sogdianite. Soviet Physics Crystallography, 19, 460–462.

Balassone, G., Boni, M., Di Maio, G. and Franco, E. (1989) Armenite in southwest Sardinia: First recorded occurrence in Italy. Neues Jahrbuch für Mineralogie Monatshefte, 1989, 49–58.

Bloss, F.D. (1981) The spindle stage: Principles and practice, 340 p. Cambridge University Press, Cambridge, England.

Buseck, P.R., and Iijima, S. (1974) High resolution electron microscopy of silicates. American Mineralogist, 59, 1–21.

Cohen, J.P., Ross, F.K., and Gibbs, G.V. (1977) An X-ray and neutron diffraction study of hydrous low-cordierite. American Mineralogist, 62, 200–202.

Enraf Nonius (1983) Structure determination package (SDP). Enraf Nonius, Delft, Holland.

Fortey, N.J., Nancarrow, P.H.A., and Gallagher, M.J. (1991) Armenite from the Middle Dalradian of Scotland. Mineralogical Magazine, 55, 135–138.

Frank, E. (1979) Celsian in leucocratic gneisses of the Berisal-complex, Central Alps, Switzerland. Schweizerische mineralogische und petrographische Mitteilungen, 59, 245–250.

Janeczek, J. (1986) Chemistry, optics and crystal growth of milarite from Strzegom, Poland. Mineralogical Magazine, 50, 271–277.

Loewenstein, W. (1954) The distribution of aluminum in the tetrahedra of silicates and aluminates. American Mineralogist, 39, 92–96.

Mason, B. (1987) Armenite from Broken Hill, Australia, with comments on calciocelsian and barium anorthite. Mineralogical Magazine, 51, 317–318.

Meagher, E.P., and Gibbs, G.V. (1977) The polymorphism of cordierite. II. The crystal structure of indialite. Canadian Mineralogist, 15, 43–49.

Medenbach, O. (1986) Ein modifiziertes Kristallbohrgerät nach Verschure (1978) zur Isolierung kleiner Einkristalle aus Dünnschliffen. Fortschritte der Mineralogie, 64, Beiheft 1, 113.

Neumann, H. (1939) Armenite, a new mineral. Norsk Geologisk Tidsskrift, 19, 312–313.

——— (1941) Armenite, a water-bearing barium-calcium-alumosilicate. Norsk Geologisk Tidsskrift, 21, 19–24.

Pouliot, G., Trudel, P., Valiquette, G., and Samson, P. (1984) Armenite-thulite-albite veins at Rémigny, Quebec: The second occurrence of armenite. Canadian Mineralogist, 22, 453–464.

Putnis, A., Fyfe, C.A., and Gobbi, G.C. (1985) Al,Si ordering in cordierite using "magic angle spinning" NMR. I. Si^{29} spectra of synthetic cordierites. Physics and Chemistry of Minerals, 12, 211–216.

Schomaker, V., and Marsh, R.E. (1983) On evaluating the standard deviation of U_{eq}. Acta Crystallographica, A39, 819–820.

Schreyer, W. (1966) Synthetische und natürliche Cordierite, III Polymorphiebeziehungen. Neues Jahrbuch für Mineralogie Abhandlungen, 105, 211–244.

Semenenko, N.P., Litvin, A.L., Sharkin, O.P., Boiko, V.L., Egorova, L.N., Shurdin, G.S., Terets, G.Ya., Savitskaya, A.B., and Ilovaiskaya, S.V. (1987) Armenite from northern Dneiper region. Mineralogicheskii Zhurnal, 9, 83–90.

Senn, Th. (1990) Ba-Gneise und Ba-Kristallisation im Gebiet der Wasenalp VS. Schweizerische Mineralogische und Petrographische Mitteilungen, 70, 167.

Sheldrick, G.M. (1976) SHELX-76. Program for crystal structure determination. University of Cambridge, Cambridge, England.

——— (1986) SHELXS-86/ Fortran-77 program for the solution of crystal structures from diffraction data. Institut für anorganische Chemie der Universität Göttingen, Germany.

Žák, L., and Obst, P. (1989) Armenite-feldspar veins in basic volcanic rocks from Chvaletice (Czechoslovakia). Casopsis pro Mineralogii a Geologii, 34, 337–351.

Manuscript received April 30, 1991
Manuscript accepted November 4, 1991